Check for updates

ADVANCED ELECTRONIC MATERIALS
www.advelectronicmat.de

Polymer-Based Composites for Engineering Organic Memristive Devices

Carlos David Prado-Socorro, Silvia Giménez-Santamarina, Lorenzo Mardegan, Luis Escalera-Moreno, Henk J. Bolink, Salvador Cardona-Serra, and Eugenio Coronado*

Memristive materials play a key role in the development of neuromorphic technology given that they can combine information processing with volatile or nonvolatile memory storage in a single computational component. Both functionalities are strictly required for the design and implementation of neuromorphic circuits. Many of these bioinspired materials emulate the characteristics of memory and learning processes that happen in the brain. The memristive properties of a two-terminal (2-T) organic device based on ionic migration mediated by an ion-transport polymer are reported here. The material possesses unique memristive properties: it is reversibly switchable, shows tens of conductive states, presents Hebbian learning demonstrated by spiking time dependent plasticity, and behaves with both short- and long-term memory in a single device. The origin and synergy of both learning phenomena are theoretically explained by means of the chemical interaction between ionic electrolytes and the ion-conductive mediator. Further discussion on the transport mechanism is included to explain the dynamic behavior of these ionic devices under a variable electric field. This polymer-based composite as an outstanding neuromorphic material is proposed for being tunable, cheap, flexible, easy to process, reproducible, and more biocompatible than their inorganic analogs.

1. Introduction

Current modern computers are built under the traditional von Neumann architecture, which is characterized by a memory-computing structure where the memory unit and the central processing unit (CPU) are physically separated. Under this architecture, the memory unit stores both data and program instructions, sharing the same data-transfer channel to the CPU.[1] The consequence is that the processor is idle for a certain amount of time while memory is accessed. This limitation is known as von Neumann bottleneck.[2] Such nondesirable effect critically limits the effective processing speed of large amounts of data, hindering the development of future AI applications such as pattern recognition and big data mining, among others. To mitigate this limitation, a variety of proposals based on non-von Neumann architectures are being explored by the scientific community. Mostly based on the idea of unifying processing and memory units, in-memory processing technologies have emerged as the most promising solution. These technologies attempt to mimic the most efficient computer in terms of processing speed, learning processes and low energy consumption: the biological brain (see **Figure 1**a). With around 20 W of power consumption, it intensively processes and classifies daily life big-data, a feat that no artificial proposal has managed to achieve up to date.[3]

One of the most promising strategies to implement neuromorphic computing requires integrating the memristor, an unconventional electronic component. Theoretically proposed by Chua et al. in 1971,[4,5] a memristor is a fundamental electronic element at the level of resistors, inductors, and capacitors, that portrays the ability of varying its intrinsic resistance depending on the previous history of voltage applied to it. Materials showing this capability are still under exhaustive exploration for developing functional memristive devices. Initially, such devices were suggested as resistive memories (ReRAM) for digital storage of information where high memory retention, linearity, and symmetry are required. However, their full potential is achieved in analog computing,[6] where the continuous variation of resistance shown by memristive devices can accurately be used to solve complex "maze-type" problems. This analog behavior has proposed to build hardware-based artificial neural-networks with specific pattern-recognition algorithms.[7–11]

The first physical characterization of a memristive device was reached with the TiO_2 memristor.[12] The mechanism is based on oxygen vacancies electroformed at the surface of a titanium dioxide layer sandwiched by two titanium electrodes.[13,14] Soon after, a variety of alternatives for obtaining new memristive mechanisms emerged. Fruitful remarkable examples include phase change memories,[15–17] metallic filament migration,[18–20] and magnetic tunnel junctions;[21–23] all of them using solid-state inorganic materials like noble metals or metal oxides. Despite the recent success of these extended inorganic materials, no large-scale commercialization has yet been achieved,

C. D. Prado-Socorro, S. Giménez-Santamarina, L. Mardegan, L. Escalera-Moreno, H. J. Bolink, S. Cardona-Serra, E. Coronado
Institute of Molecular Science
Universitat de València
C/Catedrático Jose Beltrán n 2, Paterna, Valencia 46980, Spain
E-mail: salvador.cardona@uv.es

The ORCID identification number(s) for the author(s) of this article can be found under https://doi.org/10.1002/aelm.202101192.

© 2022 The Authors. Advanced Electronic Materials published by Wiley-VCH GmbH. This is an open access article under the terms of the Creative Commons Attribution-NonCommercial-NoDerivs License, which permits use and distribution in any medium, provided the original work is properly cited, the use is non-commercial and no modifications or adaptations are made.

DOI: 10.1002/aelm.202101192

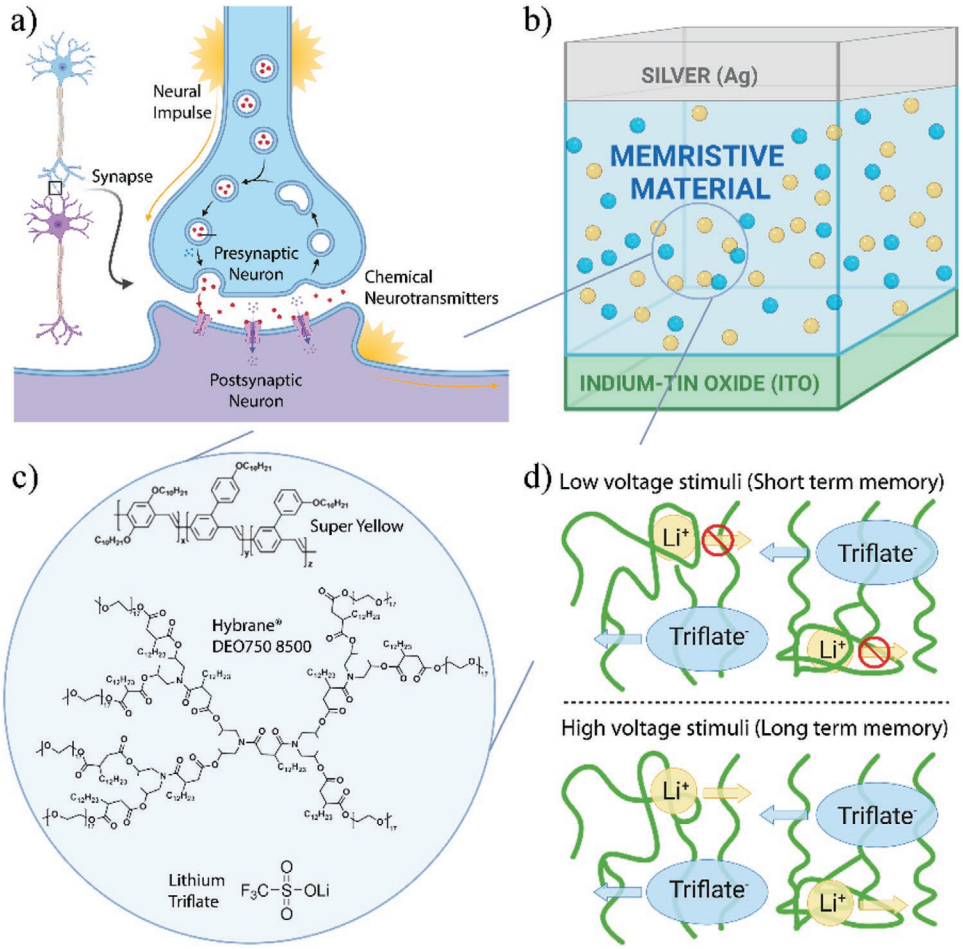

Figure 1. a) Depiction of the electrical transmission in a neural impulse: neurotransmitters are discharged into the synaptic cleft between the presynaptic and postsynaptic neurons, facilitating information transmission. b) Schematic of a single synaptic device, where, in absence of voltage, the memristive material shows homogeneous presence of ions. c) Composition of the memristive layer: Super Yellow (semiconductive polymer), Hybrane DEO750 8500 (ion-transport polymer), and lithium triflate ($LiCF_3SO_3$). d) Proposed mechanism of the origin of the short/long term memory (STM/LTM) considering the distinct mobilities of ions (blue, yellow) embedded in the polymeric matrix (green).

mostly because their memristive capabilities are inherently limited by their low chemical variability and functionalization, difficulties in nanostructuration, reduced biocompatibility, and, more importantly, poor reproducibility due to large parameter dependences.[24–26]

However, organic materials can potentially form memristive devices which excel in these aspects, as they take advantage of high versatility in molecular chemistry to design materials while reducing the size and energetic requirements.[27] These materials are also "green" and may improve the processability by means of low-cost soft techniques. Other advantages include flexibility, low power consumption, dense circuit integration, and biocompatibility, which is crucial for applications in the field of nervetronics.[28] All of these characteristics have set the focus of material chemists toward obtaining new organic memristive devices.[29–36]

One of the first attempts at this was presented by Malliaras and co-workers.[29] In this contribution, the authors published a bistable electrochemical cell with the $[Ru(bpy)_3(PF_6)_2]$ complex as active material. This device aimed to mimic the structure of the original TiO_2 memristor, but benefitting from the ionic redistribution of PF_6^- anions upon application of a bias voltage. Later, in 2014, Lei et al. tested a device consisting of a thin layer of polyvinyl alcohol in the absence of ions.[37] However, despite the novelty of including a polymeric material, Lei's work did not introduce any insight into the mechanism governing the observed memristive behavior.[37] Thus, all attempts to design and improve these devices remained so far unsuccessful, only showing "write-once, read-many" devices at best.[38] In addition, these organic devices required the use of a 3-T structure to obtain a relatively long memory remanence.[39–42] In 2016, Liu et al. achieved for the first time a device based on an organic redox system, $[EV(ClO_4)]$/(BTPA-F) showing a 2-T device which can be tuned from short-term memory (STM) to long-term memory (LTM).[43] Although this seminal contribution demonstrated the validity of organic materials for synaptic applications, the memristive redox reaction induced permanent changes in the organic layers, limiting reversibility.

In this work, we overcome such complexity by taking a step forward in the fabrication, design, and learning properties of a polymer-based composite 2-T memristive device. We aim

© 2022 The Authors. Advanced Electronic Materials published by Wiley-VCH GmbH

to obtain a reliable, robust, and totally reversible memristive behavior in an organic material.

Compared with the previous organic devices, our contribution shows remarkably better stability (10^6 s, at least one order of magnitude higher compared with other polymeric materials),[38] richer relaxation phenomenology, which includes two different memory regimes, and a relatively similar energy consumption (≈6 fJ/100 nm[2]).[34]

This proof of concept is based on a mixture of an organic conductive polymer, a solid electrolyte and an embedded salt. A similar composite has been proposed to build a light emitting electrochemical cell (LEC), where the ion transport mediated the electroluminescence of the device.[44] Including a solid electrolyte is crucial since it benefits our approach in two ways: first, its structure embodies a large concentration of polar groups on the side chains, permitting adequate solvation of the salt, which in turn maximizes the number of ionic carriers. Second, the cohesive energy of the polymer is low enough to maintain a certain flexibility, allowing for the reorientation of the local coordination geometry as well as the segmental motion of the side chains, while preferably coordinating the cations. An important novelty of our material concerns the distinct mobilities of anions and cations which are proposed to be the origin of different responses to voltage, producing two memory regimes. In this way, we selected a well-known salt (lithium triflate, $LiCF_3SO_3$) due to the large difference in charge density between its anion and cation species. We characterize the memristive behavior by means of analog conductive performance, revealing a continuous scheme of achievable and reversible states. In this way, multiple controllable hysteresis loops in the *I–V* curves are reported, along with excitatory postsynaptic current (EPSC), STM and LTM, and spike-time dependent plasticity (STDP). Additionally, the observed memristive behavior was described by a qualitative ionic migration mechanism that explained both memory regimes in terms of chemical intermolecular interactions.

2. Results and Discussion

Synaptic devices with a vertical structure (Figure 1b) were fabricated by implementing an active layer composed of a mixture of three materials: *poly[{2,5-di(30,70-dimethyloctyloxy)1,4-phenylenevinylene}-co-{3-(40-(300700-dimethyloctyloxy) phenyl)1,4phenylenevinylene}-co-{3-(30-(30,70-dimethyloctyloxy) phenyl)-1,4-phenylenevinylene}]* (Super Yellow, SY, organic semiconductor), Hybrane DEO750 8500 (ion-transport polymer), and lithium triflate ($LiCF_3SO_3$) (Figure 1c). These precursors were dissolved in cyclohexanone at a concentration of 15, 10, and 5 mg mL^{-1}, respectively, and then mixed following the mass ratio of 1:0.30:0.09 with respect to Super Yellow, ending with a final concentration of 8.72, 2.62, and 0.78 mg mL^{-1}. Prepatterned indium tin oxide (ITO) coated glass plates were used as transparent conductive substrates. After the cleaning process, the substrate was dried and the prepared solution was spun at 2000 rpm for 60 s. The as-coated films were annealed for 3 h at 75 °C to form a uniform, homogeneous thin layer. The obtained film presented a thickness of 209 nm, characterized by profilometry measurements. Topography images were taken through an atomic force microscopy (AFM) for a different spin-coating rotational speed rate (see Figures S1 and S2, Supporting Information). The top electrode (Ag, 100 nm thickness) was thermally evaporated on top of the active layer using a shadow mask. The active area of the junction is of 0.0825 cm^2. The whole fabrication procedure (i.e., preparation of solutions, spin-coating, annealing, and thermal evaporation) has been conducted under N_2-filled atmosphere to assure maximum reproducibility while avoiding contamination. The robustness of these kind of active layers has also been proved by incorporating them into light emitting electrochemical cells, which have shown long electroluminescence lifetime (≈1600 h).[44]

This chemically engineered structure was then electrically characterized to unveil the features of a memristive material, including short- and long-term memory in a single 2-T device (Figure 1d).

In a first step, current–voltage (*I–V*) curves were measured to determine its artificial synaptic nature. The current dependence on triangular voltage sweeps applied to the device produced the typical hysteretic behavior, shown in **Figure 2**a. We found that successive applications of single-polarity sweeps offer an increasing current, meaning that the conductance of the device evolves with the application of voltage in time. This process is repeatable and reversible, achieving different conductance levels, which translates in current increments at certain reading voltages being distinguishable between successive cycles. Sweeping *I–V* cycles with negative polarity produces a totally different hysteretic cycle. This has been attributed to electrochemical side-reactions occurring in the vicinity of the electrodes, which create an insulating layer. This phenomenon has already been observed in other LEC structures based on poly[2-methoxy-5-(2′-ethylhexyloxy)-1,4-phenylene vinylene].[45,46] For example, Figure 2a shows that the current increases by 140% from the first to second cycle, and at the 10th cycle, it still increases by 6.3% from the 9th cycle. In Figure 2c, a more detailed continuous evolution on the conductive properties is displayed versus a voltage pulse sequence (Figure 2b). In this case, the pulse train consisted of 50 pulses of 1 V, followed by 50 pulses of −2 V, with the conductance values measured at the pulse peaks. It is then validated that the conductance can be tuned and continuously potentiated and depotentiated by at least 200%, offering a wide range of accessible resistance states. This gradual and continuous change of the resistance is an advantage with respect to the more common resistance switching devices,[12,17] where only a few conductance states are achievable. Particularly in many organic devices, this is usually an irreversible process, behaving as "write once—read many" devices.[47]

Once we demonstrated a fine tuning of the devices' conductance, a second step consisted in unveiling the synaptic memory times of the ionic material. Here, we determine the changes in conductance obtained by a set of pulses and its time evolution by testing the EPSC (**Figure 3**a). In the EPSC measurements, a train of voltage pulses is applied to the system, allowing for a short-term relaxation between each individual pulse. With this scheme, an increasing current baseline with longer remanence can be detected. In particular, the measurements were applied as follows: first, the device was initiated on its ground state by applying V_0 = 1 V during 1 s (state S_0). Then a short presynaptic positive voltage pulse of 2 V was applied during 0.05 s

© 2022 The Authors. Advanced Electronic Materials published by Wiley-VCH GmbH

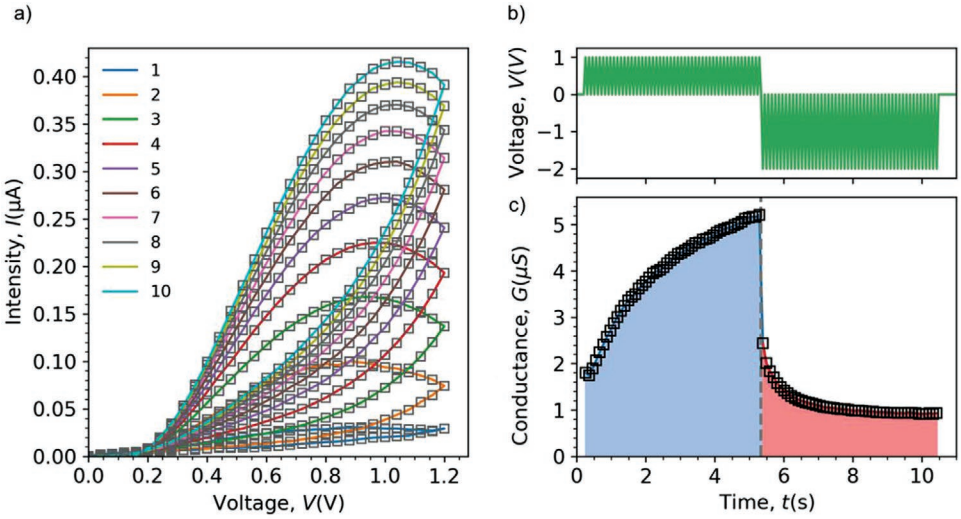

Figure 2. a) Hysteresis loops obtained by successively applying triangular voltage sweeps at a rate of 0.25 V s^{-1}, waiting 10 s between each cycle. b) Pulsed voltage sequence implemented to tune the device's conductance shown in (c). c) Learning/forgetting behavior in a single memristive device, achieved by applying the pulses shown in (b).

to start the EPSC. Subsequently, the system was left at 1 V so it spontaneously relaxes to an excited steady state (S_1) for 1 s. This sequence was repeated to achieve a second excited state (S_2). After that, two equivalent postsynaptic negative pulses of −2.5 V were applied during 0.05 s to obtain the corresponding decreased EPSC, showing states S_3 and S_4. With this simple experiment, we determined four different, easy to achieve conductive states around ground level. The EPSC ratios, measured as the conductance of an excited state (S_n) divided by that of the ground state (S_0), are 7.333, 15.553, −3.716, and −16.967 for S_1, S_2, S_3, and S_4, respectively. These values are large enough to assure differentiation in order to identify the conductance levels.

Furthermore, two extra experiments were performed to quantitatively determine the tunability of the conductance by applying a particular train of pulses. In the first test, our objective was to determine the plasticity of the material by applying a controlled number of voltage pulses. In the second test, we aimed to determine the relaxation rate of the memory states as function of certain reading time. In Figure 3b, a schematic representation of the voltage pulses for both tests is displayed. Here, a starting reading pulse (V_{read} = 0.5 V) was applied to measure the initial conductance state (G_0). This voltage was selected to be low enough to avoid ion migration, and as an indicator of the starting state of the device. Then, a sequence of pulses (N_{pulses}) was applied, maintaining V_{write} = 1 V and t_{write} = 0.1 s (time between each writing pulse). After waiting a variable amount of time (t_{wait}) with the circuit set to high impedance conditions, a second reading pulse was applied to determine the new conductance state (G_f). In either case, the conductance values were measured at the 0.5 peaks. In these measurements, a reset time of 300 s between experiments was selected, with the circuit now set to short-circuit conditions. This was done in order to guarantee a total recovery of the initial conductance state. In all cases, the variation of the device's conductance was calculated as the percentage ratio between the two reading pulses, $\frac{G_f}{G_0}\cdot 100$. Each studied variable (t_{wait}, N_{pulses}) was analyzed independently for either test.

For statistical reasons, several independent devices were measured. The dispersion of measurements was found to be low, especially at a low range of N_{pulses}, and for a long t_{wait}, demonstrating great reproducibility in a large range of parameters.

From these experiments, we conclude that the conductance of the device is susceptible to be finely controllable, gaining a wide range of achievable states with a very low energy cost (≈50 nJ per event). This is illustrated in Figure 3c, where ΔG is linearly represented versus N_{pulses} in logarithmic scale for a waiting time of t_{wait} = 150 ms. In Figure 3d, the evolution of the conductance (ΔG) versus t_{wait} is represented. In this test, two different excitatory regimes were explored: in the first one, devoted to achieve STM stimulation, V_{write} = 1 V with both N_{pulses} = 10 and N_{pulses} = 50 were set (blue, red). For the case of longer memory times, V_{write} = 3 V with N_{pulses} = 10 was found to be enough to achieve LTM. Regarding STM, an initial increase of conductance is achieved at very short times (t_{wait} < 500 ms). In LTM, the same phenomenon persists until longer times of t_{wait} < 2 s. This feature is related with the ionic movement inertia present after the applied train of pulses. However, for longer t_{wait} values we observed the expected exponential relaxation of the conduction. These decays were fitted to a modified Kohlrausch equation (see Figure S3, Supporting Information),[48] obtaining the characteristic times τ_S = 2.5–3 s for STM and τ_L = 4.7 s for LTM. Quantitatively, the retention time was extracted by analyzing at which point the increase of conductance is negligible (G_f/G_0 < 1.05). The obtained value was limited to 10–15 s for STM and more than 45 s for LTM, thus defining the open work window for sequential stimulation as well as a fine manipulation at very short times.

Moreover, an additional synaptic function called spike-timing-dependent plasticity (STDP), also known as Hebbian learning rule,[49] was tested in these devices. STDP is a synaptic function necessary to implement these materials into neuromorphic circuits capable of showing features such as artificial vision.[50] Here, the objective was to translate pulse timing differences into voltage amplitude differences. Experimentally, we

© 2022 The Authors. Advanced Electronic Materials published by Wiley-VCH GmbH

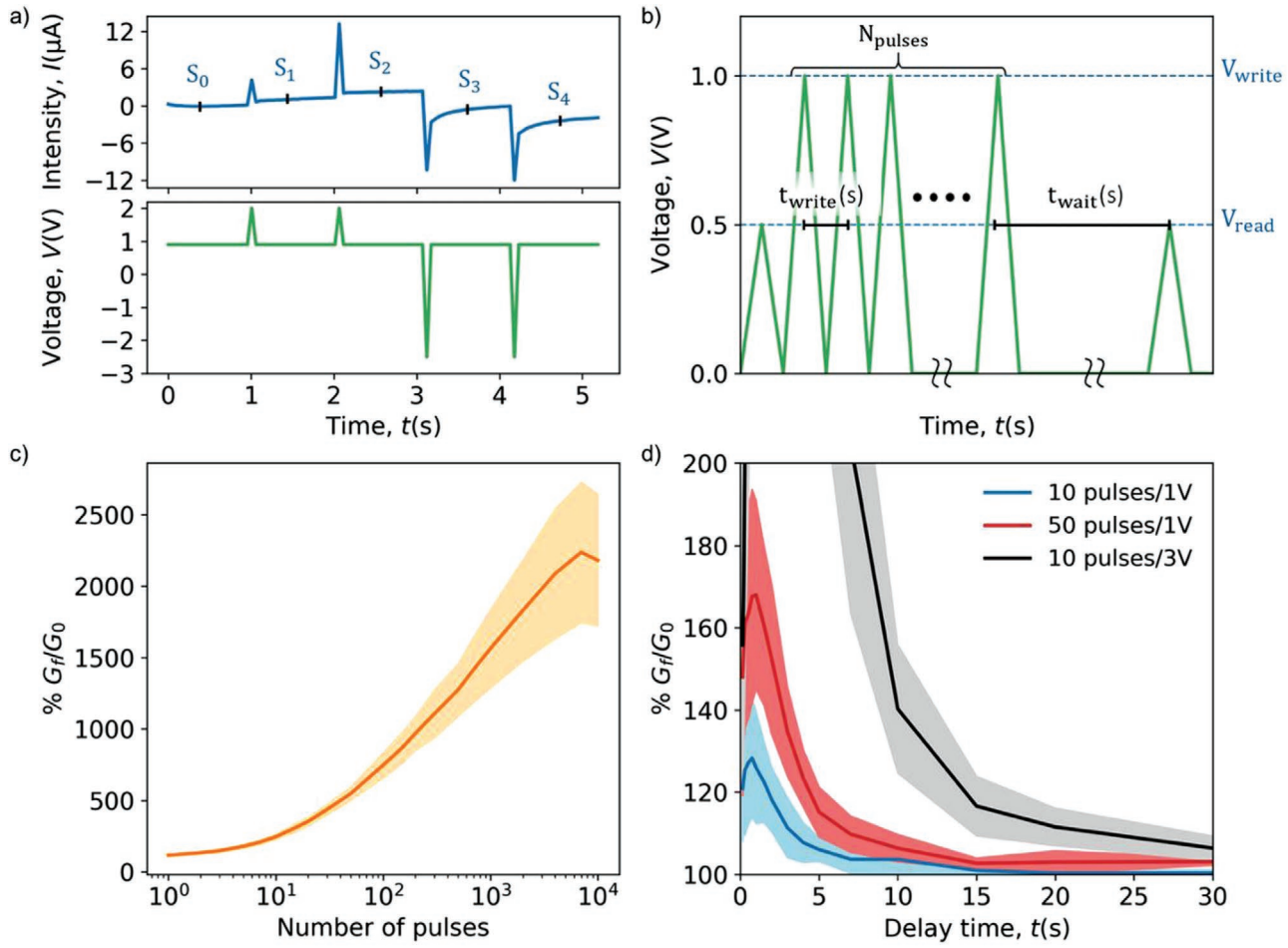

Figure 3. a) Excitatory postsynaptic current measurements, showing that either positive or negative voltage stimuli produce noticeable variations in the current (and thus, conductance) of the junction. b) Schematic representation of voltage pulses employed for the experiments shown in (c) and (d). c) Determination of conductance susceptibility ($\frac{G_f}{G_0}$.100) for a variable number of voltage pulses; the shadowed area displays the dispersion of measurements. d) Relaxation rates for short time (blue, red) and long time (black) memory states as a function of waiting time.

confirmed a change in sign and/or magnitude of the conductance with respect to the relative timing between the pre- and postelectronic spikes (**Figure 4**a). A general scheme of the pre- and postsynaptic pulses, with a maximum spiking voltage of V_{sp}, is shown in Figure 4a-inset. This means that the voltage function applied at each point of the experiment was calculated as the voltage function summation between pre- and postsynaptic pulses, which are separated by a delay of Δt (Figure 4b–d). If $\Delta t < 0$, the total synaptic pulse drives to an increase of the conductance (synaptic potentiation); otherwise, for $\Delta t > 0$, a conductance decrease is found (synaptic depression). With such a disposition of pre- and postsynaptic spikes, we chose a value for V_{sp} = 1.55 V, enough to activate ionic migration, while keeping the material safe from any electrochemical degradation. In this case, the obtained results correspond to an asymmetric anti-Hebbian learning, which was fitted to the corresponding equation for both positive and negative Δt (Equation (1))

$$\Delta G = Ae^{\frac{-\Delta t}{\tau}} + G_0 \quad (1)$$

where ΔG is the percentage of change in the device's conductance, Δt is the time difference between presynaptic and postsynaptic spikes, τ is the fitted time constant of the synaptic function, and A and G_0 are fitting constants.

In both cases, the attained value for τ is in the range of 85–90 ms. This result is in good agreement with the values previously obtained for biological synapses based on real neurons (≈100 ms).[51]

We estimated that our nonencapsulated memristive devices function properly for two weeks (≈300 working hours) after fabrication, even while resting in air at room temperature (see Figure S4, Supporting Information), showing an excellent stability for this category of devices,[52] but with room for improvement.

3. Theoretical Origin of Memristance Based on Ion Transport Mechanism

In this section, we attempt to describe the observed memristive behavior by considering a qualitative ionic migration

© 2022 The Authors. Advanced Electronic Materials published by Wiley-VCH GmbH

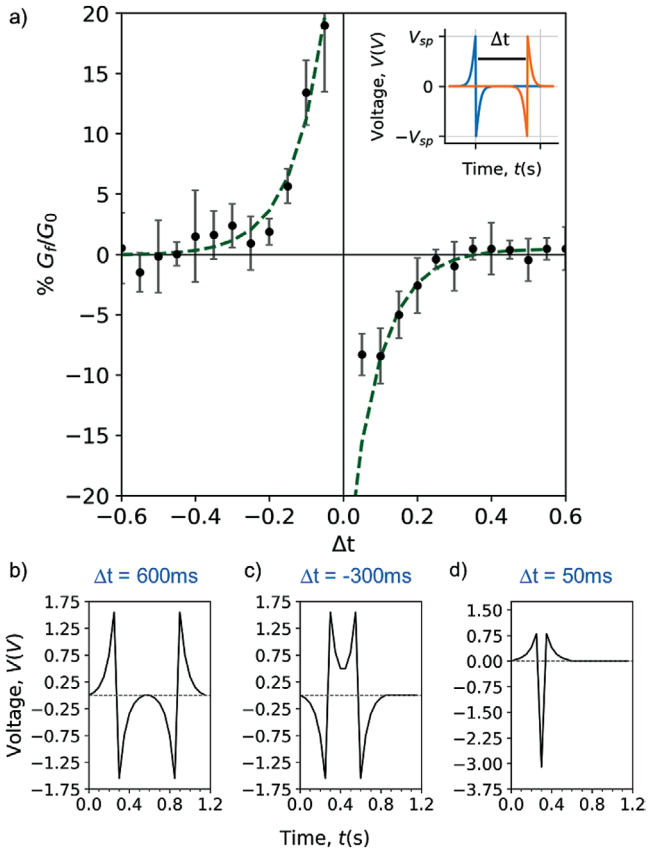

Figure 4. a) Experimentally measured STDP function (fitted to a Hebbian learning model), demonstrating the possibility of translating time-dependent pulses to conductance change. (Inset) Pre- and postsynaptic spikes separated by a delay of Δt, which served as the independent variable. b–d) Voltage function applied for Δt = 600, −300, and 50 ms, respectively.

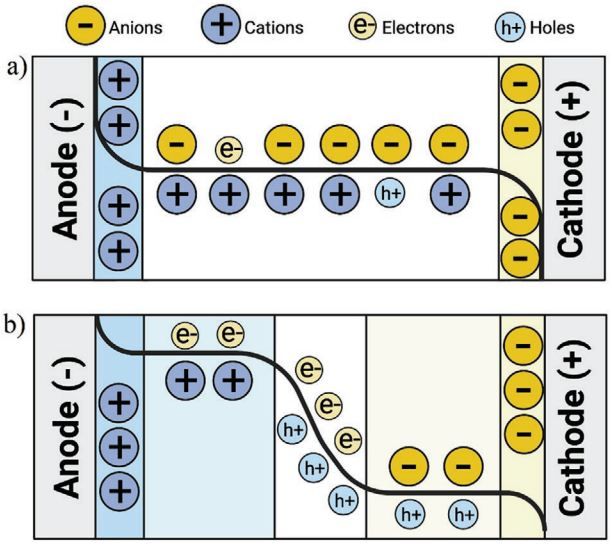

Figure 5. Schematic 1D representation of ion migration mechanisms. a) Electrodynamic model (injection-limited regime; no effective polymer doping exists). b) Electrochemical Doping model (ohmic injection regime; the polymer conductivity is modified by electronic doping).

mechanism.[53,54] Initially, in the absence of an applied voltage or current, the distribution of ions in the polymeric matrix is homogeneous and constant along the device. When a certain voltage stimulus is applied, the resulting electric field slightly alters the position of the different anions and cations, modifying the voltage profile of the device and producing a charged double layer in the vicinity of the electrodes. Thus, the nominal resistance of the device can be defined as a function of time, magnitude, and sign of the voltage applied.

In this regard, there are two mainly accepted theories to deal with the ionic movement and its effects on the electron injection.[53–58] In the Electrodynamic model,[53,54] an injection-limited regime is considered, and the majority of potential is concentrated in the vicinity of the electrodes. The presence of this ionic layer is known to effectively bend the valence and conduction bands of the polymer, diminishing the Schottky barrier that needs to be surpassed in order to inject electrons and holes. On the other hand, in the Electrochemical Doping model,[55] a reduced voltage drop occurs toward the leads due to the accumulation of ions as in the previous case. However, since the injection is considered to be ohmic in this model, the electronic doping of the polymer is permitted and, consequently, a displacement of cations and anions must occur in order to compensate the doping charges (**Figure 5**). After a strong debate, both models were shown in 2010 to represent different operations depending on the injection regime.[59]

The different mobilities in the polymeric environment between fast electrons and holes versus slow anions and cations lead to the fact that, for fast enough measuring times, the charge background and voltage profile can be considered stationary. Thus, the electron/hole injection is adjusted for each static ionic configuration. This could pave the way for modeling out-of-equilibrium states with achievable steady-state approximations.

In our case, the presence of the solid electrolyte polymer mediates both the effective mobility of the ions, and the minimum energy needed to displace them from their equilibrium positions. In this regard, we propose the ionic migration to be the key process determining the remanence times, whose magnitude depend on the interaction between the ion coordinating polymer (Hybrane DEO750 8500) and the salt ions. Basically, due to acid-base Lewis forces, the Li^+ cation (hard acid) strongly interacts with the O atoms (hard basis) present in the Hybrane structure. Therefore, only high enough voltage stimuli (i.e., 3 V) are able to promote the movement of Li^+ ions. However, this is not the case for the triflate anions. As a soft basis with less charge/surface, the salt anion is known to interact poorly with oxygen atoms from Hybrane, thus being easily displaced by a weaker bias voltage.

4. Conclusion

We have reported the material engineering and fabrication of a novel type of organic memristive device based on a conductive polymer-solid electrolyte composite. The electrical characterization in terms of postsynaptic current (EPSC) and

© 2022 The Authors. Advanced Electronic Materials published by Wiley-VCH GmbH

neural plasticity (STDP) offered values in close agreement with their biological counterparts. Our contribution states that the Coulomb interactions between the solid electrolyte and solvated ions point toward two ion conduction regimes, which probably are at the origin of the coexistence of STM (10–15 s) with LTM (>45 s) in a single 2-T device. Using such a simplified structure is a clear advantage in processability and energy consumption compared to previous 3-T attempts in organic devices. Finally, the continuous variation in the conductance of the material has been explained by adapting the theoretical models previously developed for electrochemical cells. Within these mechanisms, memristivity is naturally arising from the continuous displacement of ions, and eventually, from certain polymer doping, depending on the injection regime.

The above results show that our ion-polymer material can be successfully used for the development of artificial synaptic devices in which the conductance of the junctions can be finely manipulated, obtaining a quasi-continuous analogic behavior with a low power consumption (≈50 nJ per event) and complete reversibility. This is a key improvement from the previous inorganic contributions where low reproducibility only allows to obtain a digital switchable device with a low number of achievable conductance levels. Yet, while the robustness of these organic devices is higher than those reached in other organic proposals, it is still lower than that of the inorganic counterparts.

To improve the robustness of our devices, further work will be developed based on chemical tailoring. This chemical design is expected to offer, in addition, larger memory times and faster, lower energy-demanding synaptic operations.

5. Experimental Section

Materials: The semiconducting polymer (SY), $LiCF_3SO_3$, and cyclohexanone were purchased from Merck and Hybrane DEO750 8500 from Polymer Factory. All reagents were used without any further treatment.

Solution Preparation: SY, Hybrane and $LiCF_3SO_3$ were dissolved in cyclohexanone at a concentration of 15, 10, and 5 mg mL^{-1}, respectively, after which the SY solution was left under continuous stirring at 50 °C overnight. They were later mixed following the mass ratio of 1:0.30:0.09 with respect to SY, ending with a final concentration of 8.72, 2.62, and 0.78 mg mL^{-1}. This process was performed in a N_2-filled atmosphere.

Device Preparation: ITO-patterned substrates were washed ultrasonically in water-soap (Mucasol), water, and 2-propanol baths before putting them inside a glovebox. Then, they were dried with a N_2 gun, and the 60 s, 2000 rpm spin-coating process was performed with the prepared solution. Once the active material had been deposited, the substrates were annealed at 75 °C for 3 h. Subsequently, 100 nm of Ag was evaporated on top of the active layer using a shadow mask. The whole process (excluding the initial substrate washing) was performed in a N_2-filled atmosphere. (Optical images of a standard device are provided in Figure S5, Supporting Information.)

Profilometry Characterization and AFM Imaging: The thickness of the deposited active layer was determined with the Ambios XP-1 profilometer. The AFM imaging was performed with the Bruker Dimension Icon AFM set in tapping mode. The tip used was of silicon with a resonant frequency of 300 kHz and a force constant of 40 N m^{-1}. The scan rate was of 0.6 Hz. Both studies were performed in air under room temperature. Devices employed for these studies were not electrically characterized.

Electrical Characterization: Devices were electrically characterized using a Keithley 2450 SourceMeter and self-made programming code written in the Keithley Test Script Builder. The devices remained in a N_2-filled atmosphere during the whole procedure, except for the case of some degradation studies.

Supporting Information

Supporting Information is available from the Wiley Online Library or from the author.

Acknowledgements

The research reported here was supported by the Spanish MINECO (Excellence Unit María de Maeztu CEX2019–000919-M), the European Union (ERC-AdG MOL2D 788222 and ERC AdG HELD 834431), the Generalitat Valenciana (Prometeo Program of Excellence), and the Universitat de València (PRECOMP14-202646). S.C.-S. thanks the Spanish MINECO for a "Juan de la Cierva-Incorporación" grant, S.G.-S acknowledges the Spanish Ministry of Education (grant PRE2018-083350), C.D.P.-S. thanks the Spanish Ministerio de Asuntos Económicos y Transformación Digital (MINECO) for a Predoctoral Grant (PRE2020-093666). The authors also thank Denissé de Dios Torralba, Angel López and Alejandra Soriano for their experimental support. Finally, the authors thank Michele Sessolo for his useful advice about LECs.

Conflict of Interest

The authors declare no conflict of interest.

Data Availability Statement

The data that support the findings of this study are available from the corresponding author upon reasonable request.

Keywords

electroactive materials, electrochemical cells, memristive materials, memristors, molecule-based materials, organic electronics, organic semiconductor, polymeric materials

Received: November 22, 2021
Published online:

[1] J. Von Neumann, *IEEE Ann. Hist. Comput.* **1993**, *15*, 27.
[2] Editorial, *Nature* **2018**, *554*, 145, https://www.nature.com/articles/d41586-018-01683-1.
[3] D. Drubach, The Brain Explained, Prentice Hall, **2000**.
[4] L. Chua, *IEEE Trans. Circuit Theory* **1971**, *18*, 507.
[5] M. Prezioso, F. Merrikh-Bayat, B. Hoskins, G. C. Adam, K. K. Likharev, D. B. Strukov, *Nature* **2015**, *521*, 61.
[6] Y. V. Pershin, M. Di Ventra, *IEEE Trans. Circuits Syst. I Regul. Pap.* **2010**, *57*, 1857.
[7] A. Mizrahi, T. Hirtzlin, A. Fukushima, H. Kubota, S. Yuasa, J. Grollier, D. Querlioz, *Nat. Commun.* **2018**, *9*, 1533.
[8] D. Vodenicarevic, N. Locatelli, J. Grollier, D. Querlioz, *J. Appl. Phys.* **2018**, *124*, 152117.

© 2022 The Authors. Advanced Electronic Materials published by Wiley-VCH GmbH

[9] F. L. Traversa, C. Ramella, F. Bonani, M. Di Ventra, *Sci. Adv.* **2015**, *1*, e1500031.
[10] F. L. Traversa, M. Di Ventra, *IEEE Trans. Neural Networks Learn. Syst.* **2015**, *26*, 2702.
[11] E. J. Fuller, S. T. Keene, A. Melianas, Z. Wang, S. Agarwal, Y. Li, Y. Tuchman, C. D. James, M. J. Marinella, J. J. Yang, A. Salleo, A. A. Talin, *Science* **2019**, *364*, 570.
[12] D. B. Strukov, G. S. Snider, D. R. Stewart, R. S. Williams, *Nature* **2008**, *453*, 80.
[13] J. J. Yang, M. D. Pickett, X. Li, D. Ohlberg, D. R. Stewart, R. S. Williams, *Nat. Nanotechnol.* **2008**, *3*, 429.
[14] M. D. Pickett, D. B. Strukov, J. L. Borghetti, J. J. Yang, G. S. Snider, D. R. Stewart, R. S. Williams, *J. Appl. Phys.* **2009**, *106*, 074508.
[15] W. W. Koelmans, A. Sebastian, V. P. Jonnalagadda, D. Krebs, L. Dellmann, E. Eleftheriou, *Nat. Commun.* **2015**, *6*, 8181.
[16] M. L.e Gallo, A. Sebastian, R. Mathis, M. Manica, H. Giefers, T. Tuma, C. Bekas, A. Curioni, E. Eleftheriou, *Nat. Electron.* **2018**, *1*, 246.
[17] A. Sebastian, M. L.e Gallo, D. Krebs, *Nat. Commun.* **2014**, *5*, 4314.
[18] M. Yang, X. Zhao, Q. Tang, N. Cui, Z. Wang, Y. Tong, Y. Liu, *Nanoscale* **2018**, *10*, 18135.
[19] M. K. Kim, J. S. Lee, *ACS Appl. Mater. Interfaces* **2018**, *10*, 10280.
[20] S. H. Lee, H. L. Park, C. M. Keum, I. H. Lee, M. H. Kim, S. D. Lee, *Phys. Status Solidi RRL* **2019**, *13*, 1900044.
[21] J. Torrejon, M. Riou, F. A. Araujo, S. Tsunegi, G. Khalsa, D. Querlioz, P. Bortolotti, V. Cros, K. Yakushiji, A. Fukushima, *Nature* **2017**, *547*, 428.
[22] A. Chanthbouala, A. Crassous, V. Garcia, K. Bouzehouane, S. Fusil, X. Moya, J. Allibe, B. Dlubak, J. Grollier, S. Xavier, *Nat. Nanotechnol.* **2012**, *7*, 101.
[23] M. Romera, P. Talatchian, S. Tsunegi, F. A. Araujo, V. Cros, P. Bortolotti, J. Trastoy, K. Yakushiji, A. Fukushima, H. Kubota, *Nature* **2018**, *563*, 230.
[24] B. Mohammad, M. Abi Jaoude, V. Kumar, D. M. Al Homouz, H. A. Nahla, M. Al-Qutayri, N. Christoforou, *Nanotechnol. Rev.* **2016**, *5*, 311.
[25] Y. Li, Z. Wang, R. Midya, Q. Xia, J. J. Yang, *J. Phys. D: Appl. Phys.* **2018**, *51*, 503002.
[26] W. Sun, B. Gao, M. Chi, Q. Xia, J. J. Yang, H. Qian, H. Wu, *Nat. Commun.* **2019**, *10*, 3453.
[27] Y. Van De Burgt, A. Melianas, S. T. Keene, G. Malliaras, A. Salleo, *Nat. Electron.* **2018**, *1*, 386.
[28] H. Park, Y. Lee, N. Kim, D. Seo, G. Go, T. Lee, *Adv. Mater.* **2020**, *32*, 1903558.
[29] A. A. Zakhidov, B. Jung, J. D. Slinker, H. D. Abruña, G. G. Malliaras, *Org. Electron.* **2010**, *11*, 150.
[30] S. Goswami, A. J. Matula, S. P. Rath, S. Hedström, S. Saha, M. Annamalai, D. Sengupta, A. Patra, S. Ghosh, H. Jani, S. Sarkar, M. R. Motapothula, C. A. Nijhuis, J. Martin, S. Goswami, V. S. Batista, T. Venkatesan, *Nat. Mater.* **2017**, *16*, 1216.
[31] S. Goswami, S. P. Rath, D. Thompson, S. Hedström, M. Annamalai, R. Pramanick, B. R. Ilic, S. Sarkar, S. Hooda, C. A. Nijhuiset, *Nat. Nanotechnol.* **2020**, *15*, 380.
[32] Y. Kim, A. Chortos, W. Xu, Y. Liu, J. Y. Oh, D. Son, J. Kang, A. M. Foudeh, C. Zhu, Y. Lee, S. Niu, J. Liu, R. Pfattner, Z. Bao, T. W. Lee, *Science* **2018**, *360*, 998.
[33] D. G. Seo, Y. Lee, G. T. Go, M. Pei, S. Jung, Y. H. Jeong, W. Lee, H. L. Park, S. W. Kim, H. Yang, C. Yang, T. W. Lee, *Nano Energy* **2019**, *65*, 104035.
[34] Z. Xiao, J. Huang, *Adv. Electron. Mater.* **2016**, *2*, 1600100.
[35] Y. Van De Burgt, A. Melianas, S. T. Keene, G. Malliaras, A. Salleo, *Nat. Electron.* **2018**, *1*, 386.
[36] Y. Van De Burgt, E. Lubberman, E. J. Fuller, S. T. Keene, G. C. Faria, S. Agarwal, M. J. Marinella, A. Alec Talin, A. Salleo, *Nat. Mater.* **2017**, *16*, 414.
[37] Y. Lei, Y. Lui, X. Gao, B. Xu, S. Wang, J. Yin, Z. Liu, *AIP Adv.* **2014**, *4*, 077105.
[38] C. C. Shih, C. W. Huang, M. Gao, C. C. Chueh, C. W. Chen, *J. Mater. Chem. C* **2017**, *5*, 11421.
[39] P. Gkoupidenis, N. Schaefer, B. Garlan, G. G. Malliaras, *Adv. Mater.* **2015**, *27*, 7176
[40] W. Xu, S. Y. Min, H. Hwang, T. W. Lee, *Sci. Adv.* **2016**, *2*, e1501326
[41] Y. Fu, L. A. Kong, Y. Chen, J. Wang, C. Qian, Y. Yuan, J. Sun, Y. Gao, Q. Wan, *ACS Appl. Mater. Interfaces* **2018**, *10*, 26443
[42] P. Gkoupidenis, D. A. Koutsouras, G. G. Malliaras, *Nat. Commun.* **2017**, *8*, 15448.
[43] C. W. G. Liu, W. Zhang, L. Pan, C. Zhang, X. Yang, F. Fan, Y. Chen, R.-W. Li, *Adv. Electron. Mater.* **2016**, *2*, 1500298.
[44] L. Mardegan, C. Dreessen, M. Sessolo, D. Tordera, H. Bolink, *Adv. Funct. Mater.* **2021**, *31*, 2104249.
[45] T. Wågberg, P. R. Hania, N. D. Robinson, J. H. Shin, P. Matyba, L. Edman, *Adv. Mater.* **2008**, *20*, 1744.
[46] J. Fang, P. Matyba, N. D. Robinson, L. Edman, *J. Am. Chem. Soc.* **2008**, *130*, 4562.
[47] Q. F. Gu, J. H. He, D. Y. Chen, H. L. Dong, Y. Y. Li, H. Li, Q. F. Xu, J. M. Lu, *Adv. Mater.* **2015**, *27*, 5968.
[48] B. Sturman, E. Podivilov, M. Gorkunov, *Phys. Rev. Lett.* **2003**, *91*, 176602.
[49] D. O. Hebb, *The Organization of Behavior: A Neurophychological Theory*, Wiley, New York **1949**.
[50] O. Bichler, D. Querlioz, S. J. Thorpe, J. P. Bourgoin, C. Gamrat, *Neural Networks* **2012**, *32*, 339.
[51] D. Kuzum, S. Yu, H. P. Wong, *Nanotechnology* **2013**, *24*, 382001.
[52] L. Edman, T. Wagberg, P. R. Hania, N. D. Robinson, J. H. Shin, P. Matyba, *Adv. Mater.* **2008**, *20*, 1744.
[53] J. C. deMello, N. Tessler, S. C. Graham, R. H. Friend, *Phys. Rev. B* **1998**, *57*, 12951.
[54] J. C. deMello, *Phys. Rev. B* **2002**, *66*, 235210.
[55] Q. Pei, G. Yu, C. Zhang, Y. Yang, A. J. Heeger, *Science* **1995**, *269*, 1086.
[56] D. L. Smith, *J. Appl. Phys.* **1997**, *81*, 2869.
[57] P. Matyba, K. Maturova, M. Kemerink, N. D. Robinson, L. Edman, *Nat. Mater.* **2009**, *8*, 672.
[58] C. V. Hoven, H. Wang, M. Elbing, L. Garner, D. Winkelhaus, G. C. Bazan, *Nat. Mater.* **2010**, *9*, 249.
[59] S. van Reenen, P. Matyba, A. Dzwilewski, R. A. J. Janssen, L. Edman, M. Kemerink, *J. Am. Chem. Soc.* **2010**, *132*, 13776.

© 2022 The Authors. Advanced Electronic Materials published by Wiley-VCH GmbH